Proceedings of the XII International Symposium on Dynamic Problems of Mechanics (DINAME 2007),
P.S.Varoto and M.A.Trindade (editors), ABCM, Ilhabela, SP, Brazil, February 26 - March 2, 2007

Time-marching Aeroelastic Analysis of Typical Sections With Structural Nonlinearities in Transonic Regime

E. Camilo[1], **F. D. Marques**[1], **and J. L. F. Azevedo** [2]

[1] University of Sao Paulo/USP- Engineering School of Sao Carlos/EESC, Av. Trabalhador Saocarlense, 400, 13566-590 - Sao Carlos - SP, Brazil

[2] Aerospace Technical Center, Aeronautics and Space Institute - CTA/IAE/ASE-N 12228-904 - Sao Jose dos Campos - SP, Brazil- Sao J. dos Campos - SP, Brazil

Abstract: The application of time domain analysis for aeroelastic problem in a transonic flow is considered. The methodology here proposed is to present an investigation on the effects of nonlinearities on aeroelastic behavior for an airfoil moving in pitch and plunge. Here structural dynamics is considered in terms of free-play nonlinearities. The CFD tool employed in the present work is based on the Euler formulation. The governing equations are integrated by cell-centered, finite-volume, centered space discretization and five-stage, hybrid, explicit, Runge-Kutta time marching scheme. This CFD tool solves flows around two-dimensional lifting surfaces moving in pitch and plunge. The computational domain is discretized using unstructured grids and the movement is modeled with dynamic mesh algorithm. To solve the aeroelastic problem the Runge-Kutta method is applied combined with the CFD code. The time domain aeroelastic responses concerned particularly the NACA0012 airfoil are analysed by investigating flutter boundary and typical LCO nonlinear effects from phase plane.

Keywords: nonlinear aeroelasticity, CFD methods, transonic flows, flutter boundary, LCO.

NOMENCLATURE

a = location of elastic axis
e = total energy
k_w = typical section bending stiffness
k_α = typical section torsional stiffness
k = reduced frequency
M = Mach number
m = mass per unit span
p = pressure
$\mathbf{Q}$ = vector of generalized forces
$\mathbf{q}$ = vector of generalized coordinates
r_α = nondimensional radius of gyration about elastic axis
t = time
U_∞ = freestream velocity at upstream infinity
U^* = reduced velocity
u, v = velocities in x, y directions
w = plunge displacement at elastic axis, positive down
x_α = nondimensional c.g.-elastic axis offset

Greek Symbols

α = torsional deflection, positive nose up
α_s = torsional free-play
γ = ratio of specific heats
μ = mass ratio
ρ = air density
τ = nondimensional time
ϕ =vector of generalized coordinates
$\bar{\omega}$ = frequency ratio
ω_w = uncoupled frequency in bending
ω_α = uncoupled frequency in torsion

INTRODUCTION

In the last decades, nonlinear dynamics analysis has been largely developed and explored, both in the theorical and experimental point of view, in a vast diversity of fields in science and engineering. Nonlinear aeroelasticity is a multidisciplinary field, that is very important in aeronautics and aerospace engineering (Dowell and Tang, 2002; Dowell, Tang and Strganac, 2003). Most aeroelastic analysis of flight vehicles have been performed under the assumption of linearity. Under this assumption, the characteristics of flutter and divergence can be obtained. However, the influence of nonlinearities on modern aircraft is becoming increasingly important and the requirement for more accurate predictive tools grows stronger (Lee, Price and Wong, 1999).

Aerodynamic nonlinearity is associated with the presence of shock waves in transonic flows. In this situation, the unsteady forces generated by motion of the shock wave have been shown to destabilize single degree-of-freedom airfoil pitching motion and affect the bending-torsional flutter by lowering the flutter speed at the so-called transonic dip phenomenon (Thomas, Dowell and Hall, 2002).

Computational aeroelasticity is a relatively new field emphatisizing those types of aeroelastic problems where loads based on Computational Fluid Dynamics (CFD), which can be both unsteady and nonlinear, are used (Oliveira, 1993; Dubuc et al., 1997; Simoes and Azevedo, 1999). A significant amount of effort devoted toward the numerical solution of transonic aeroelastic phenomena, not only in the prediction of transonic dip effects (Morton, 1996; Morton and Beran, 1999; Badcock, Woodgate and Richards, 2004, 2005), but also toward that of limit cycle oscillations (LCOs). Euler

and Navier-Stokes schemes have been coupled with structural models (CSD) (Alonso and Jameson, 1994; Kousen and Bendiksen, 1994).

The methodology here presented (Alonso and Jameson, 1994; Kousen and Bendiksen, 1994) is applied to obtain the time domain aeroelastic responses for an airfoil moving in pitch and plunge in the transonic regime. The CFD tool for the solution of 2D transonic flowfield around an airfoil. has been achieved in cooperation with CTA/IAE group (Azevedo 1992; Oliveira, 1993; Bigarella, Basso and Azevedo, 2004; Simoes and Azevedo, 1999). This CFD tool has been tested and developed for the several unsteady aerodynamic applications considered in the CTA/IAE. However this CFD tool had never used for time domain aeroelastic analysis before.

Limit cycle oscillations has been previously observed in nonlinear time-marching aeroelastic solver in the transonic regime (Camilo, Marques and Azevedo, 2005,2006). In this article, the typical section model has been modified to include the structural nonlinearity of free-play in the torsional degree of freedom (DOF). The purpose of this article is to present preliminary results showing the effects of free-play on observed limit cycle behavior in the transonic regime, where aerodynamic nonlinearities are presented. Structural nonlinearities can also lead to LCO whether the flow is transonic or not. However, the present understanding of LCO induced by aerodynamic nonlinearities is less complete, and no systematic quantitative correlation between theory and experiment has been achieved (Thomas, Dowell and Hall, 2002).

In the CFD code the Euler equations are integrated by cell-centered, finite-volume, centered space discretization and five-stage, hybrid, explicit, Runge-Kutta time marching scheme. This CFD tool solves flows around two-dimensional lifting surfaces moving in pitch and plunge. The computational domain is discretized using unstructured grids and the movement is modeled with dynamic mesh algorithm. To solve the aeroelastic problem the Runge-Kutta method is applied combined with the CFD code. The time domain aeroelastic responses concerned particularly the NACA0012 airfoil are analysed by investigating flutter boundary and typical nonlinear effects like LCO from phase plane. To illustrate the performance of the CFD-CSD solver flutter boundaries for a NACA0012 airfoil is performed using structural parameters presented in Badcock, Woodgate and Richards (2004).

Aerodynamic Simulation

In the present study, the flow was assumed to be governed by the two-dimensional, time-dependent Euler equations, which may be written in integral form for Cartesian coordinates as:

$$\frac{\partial}{\partial t}\int\int_{\mathbf{V}} \mathbf{Q}dxdy + \int_{\mathbf{S}} (\mathbf{E}dy - \mathbf{F}dx) = 0, \tag{1}$$

where $\mathbf{V}$ represents the area of the control volume and $\mathbf{S}$ is its boundary, $\mathbf{Q}$ is the vector of conserved quantities and the inviscid flux vectors, $\mathbf{E}$ and $\mathbf{F}$, are given by:

$$\mathbf{Q} = \begin{bmatrix} \rho \\ \rho u \\ \rho v \\ e \end{bmatrix}, \qquad \mathbf{E} = \begin{bmatrix} \rho U \\ \rho uU + p \\ \rho vU \\ (e+p)U + x_t p \end{bmatrix}, \qquad \mathbf{F} = \begin{bmatrix} \rho V \\ \rho Vu \\ \rho Vv + p \\ (e+p)V + y_t p \end{bmatrix}. \tag{2}$$

where ρ, u, v, p and e are density, the two Cartesian components of the velocity, the pressure, and the specific total energy, respectively.

The contravariant velocity components are defined as:

$$U = u - x_t, \qquad V = v - y_t, \tag{3}$$

where x_t and y_t represents the Cartesian velocity components of the mesh.

Pressure is represented by the following state equation:

$$p = (\gamma - 1)[e - \frac{1}{2}\rho(u^2 + v^2)] \tag{4}$$

where γ is the ratio of specific heats.

The Euler equations can be rewritten for each *i-th* control volume as:

$$\frac{\partial}{\partial t}(V_i \mathbf{Q}_i) + \int_{S_i} (\mathbf{E}dy - \mathbf{F}dx) = 0. \tag{5}$$

The Euler equations are a set of nondissipative hyperbolic conservation laws. Hence, their numerical solution requires the introduction of artificial dissipation terms in order to avoid oscillations near shock waves and to damp high frequency

uncoupled error modes. The numerical dissipation terms are formed as a careful blend of undivided Laplacian and biharmonic operators (Simoes and Azevedo, 1999). Hence, the artificial dissipation operator, D_i, can be written as,

$$D_i = d^2(\mathbf{Q}_i) - d^4(\mathbf{Q}_i), \tag{6}$$

where $d^2(\mathbf{Q}_i)$ represents the contribution of the undivided Laplacian operator, and $d^4(\mathbf{Q}_i)$ the contribution of the biharmonic operator (Jameson, Schmidt and Turkel, 1981). The biharmonic operator is responsible for providing the background dissipation to damp high frequency uncoupled error modes and the undivided Laplacian artificial dissipation operator prevents oscillations near shock waves (Bigarella, Basso and Azevedo, 2004).

Therefore, the Euler equations after be fully discretized in space and the explicit addition of artificial dissipation terms, can be written as:

$$\frac{d}{dt}(V_i\mathbf{Q}_i) + C(\mathbf{Q}_i) - D(\mathbf{Q}_i) = 0, \tag{7}$$

where $C(\mathbf{Q}_i)$ represents convective operator, given by:

$$\int_{S_i} (\mathbf{E}dy - \mathbf{F}dx) \approx C(\mathbf{Q}_i) = \sum_{k=1}^{3} \left[\mathbf{E}(\mathbf{Q}_{ik})(y_{k2} - y_{k1}) - \mathbf{F}(\mathbf{Q}_{ik})(x_{k2} - x_{k1})\right],$$

where

$$\mathbf{Q}_{ik} = \frac{1}{2}(\mathbf{Q}_i + \mathbf{Q}_k), \tag{8}$$

and the (x_{k1}, y_{k1}) and (x_{k2}, y_{k2}) are vertices which define the interface between the volumes i and k.

The unsteady Euler code is based on Jamenson's finite volume and Runge-Kutta time-marching using a second-order accurate, 5-stage, explicit, hybrid scheme. The 2-D Euler equations in integral form are discretized by a finite volume procedure in an unstructured mesh (Oliveira, 1993).

Equations of Motion

Consider a typical two-degrees-of-freedom (DOF) airfoil section as shown in Fig.1. The equations of motion of this aeroelastic system can be written in the form (Bisplinghoff, et al., 1996):

$$m\ddot{w} - S_\alpha\ddot{\alpha} + \bar{G}(w) = -L, \tag{9}$$

$$-S_\alpha\ddot{w} + I_\alpha\ddot{\alpha} + \bar{M}(\alpha) = M_{ea}. \tag{10}$$

where the right-hand-side terms represent the aerodynamic loading terms, which are obtained from CFD code. The left-hand-side terms m, S and I_α are the airfoil mass, airfoil static moment and pitch axis moment of inertia about elastic axis, respectively. $\bar{G}(w) = k_w w$ and $\bar{M}(\alpha) = k_\alpha \alpha$ are the plunge and pitch stiffness terms. The equations of motion (Eqs. (9) and (10)) are adimensionalized, where the pitching and plunging stiffnesses are modeled by linear springs attached at the elastic axis. The plunge displacement is nondimensionalized with respect to the airfoil semichord b. The relevant nondimensional parameters for the coupled problem are the elastic axis location a, the radius of gyration about the elastic axis r_α, the offset between the center of mass and the elastic axis x_α the mass ration $m = \mu\pi\rho b^2$, the frequency ratio $\bar{\omega} = \frac{\omega_w}{\omega_\alpha}$ of the uncoupled natural frequency in plunge to that in pitch, and the reduced velocity $\bar{U} = \frac{U_\infty}{b\omega_\alpha}$. In addition, time is nondimensionalized with respect to the uncoupled natural frequency of the structure in pitch, i. e., $\tau = \omega_\alpha t$.

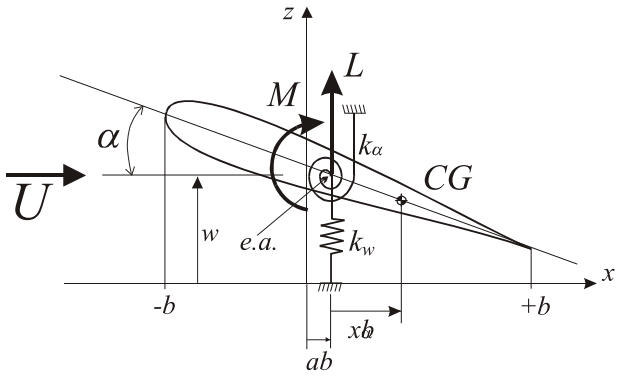

Figure 1 – Typical section model.

In terms of these dimensionless quantities, the equations of motion for the aeroelastic system are:

$$\frac{\ddot{w}}{b} - x_\alpha \ddot{\alpha} + \frac{\bar{\omega}^2}{\bar{U}^2}\frac{w}{b} = \frac{C_L}{\mu\pi}, \tag{11}$$

$$-\frac{x_\alpha}{r_\alpha^2}\frac{\ddot{w}}{b} + \ddot{\alpha} + \frac{1}{\bar{U}^2}\alpha = \frac{2C_m}{r_\alpha^2 \mu\pi}. \tag{12}$$

where C_L and C_m are nondimensional lift and moment aerodynamic coefficients, respectively.

The aeroelastic system given by Eqs. (11) and (12) are rewritten as a system of first-order differential equations by setting:

$$\phi_1 = \frac{w}{b}; \quad \phi_2 = \frac{\dot{w}}{b}; \quad \phi_3 = \alpha; \quad \phi_4 = \dot{\alpha}, \tag{13}$$

where the system of aeroelastic is expressed as:

$$\dot{\phi} = \mathbf{M^{-1}P} - \mathbf{M^{-1}K}\phi \tag{14}$$

where

$$\phi = \begin{bmatrix} \phi_1 \\ \phi_2 \\ \phi_3 \\ \phi_4 \end{bmatrix}, \quad \mathbf{P} = \begin{bmatrix} 0 \\ \frac{(U^*)^2 C_L}{\mu\pi} \\ 0 \\ \frac{2(U^*)^2 C_m}{\mu\pi} \end{bmatrix}, \quad \mathbf{M} = \begin{bmatrix} 1 & 0 & 0 & 0 \\ 0 & 1 & 0 & -x_\alpha \\ 0 & 0 & 1 & 0 \\ 0 & -x_\alpha & 0 & r_\alpha^2 \end{bmatrix}, \quad \mathbf{K} = \begin{bmatrix} 0 & -1 & 0 & 0 \\ \bar{\omega}^2 & 0 & 0 & 0 \\ 0 & 0 & 0 & -1 \\ 0 & 0 & r_\alpha^2 & 0 \end{bmatrix}. \tag{15}$$

The fourth-order Runge-Kutta time-stepping scheme is used for the time integration differential aeroelastic equations (Eqs. (15)).

Torsional Free-play

Several classes of nonlinear stiffness contributions have been studied in papers treating the open-loop dynamics of aeroelastic system (Ko, Kurdila, Strganac, 1997; Lee, Price and Wong, 1999; Liu et al., 2001). In this work, torsional

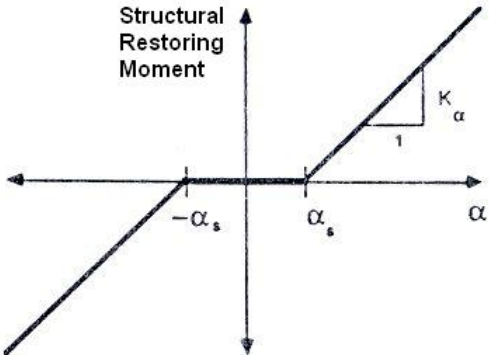

Figure 2 – Torsional Free-play.

free-play has been included in the present model, which could represent a loose hinge or linkage backlash in a control system (Kousen and Bendiksen, 1994). Then, the linear torsional moment function is replaced by the nonlinear function shown in Fig.2. Any pitch displacement between $-\alpha_s$ and $+\alpha_s$ would result in a torsional resistence of 0. Free-play modifies the aeroelastic equations of motion by changing Eq. (12) to:

$$-\frac{x_\alpha}{r_\alpha^2}\frac{\ddot{w}}{b} + \ddot{\alpha} + \frac{1}{\bar{U}^2} f(\alpha) = \frac{2C_m}{r_\alpha^2 \mu\pi}. \tag{16}$$

where the $f(\alpha)$ is given by:

$$\begin{cases} f(\alpha) = \alpha - \alpha_s & \alpha > \alpha_s \\ f(\alpha) = 0 \quad -\alpha_s < \alpha < \alpha_s \\ f(\alpha) = \alpha + \alpha_s & \alpha < -\alpha_s \end{cases} \tag{17}$$

RESULTS

To check the unsteady CFD code and mesh refinement, three AGARD test cases listed in Tab. 1 were considered. Results are shown in terms of instantaneous pressure distributions for test case 1 given in Fig. 3 for eight different incidences during the cycles. Relatively good agreement is obtained compared to the experimental values. Some minor discrepancies can be observed around the shock location at the high incidence.

Table 1 – AGARD test cases examined in this report.

Case	Airfoil	M_∞	α_m	α_0	k	a
CT1	NACA0012	0.6	2.89^0	2.41^0	0.0808	-0.237
CT2	NACA0012	0.6	3.16^0	4.59^0	0.0811	-0.237
CT3	NACA0012	0.755	0.016	2.51^0	0.0814	-0.25

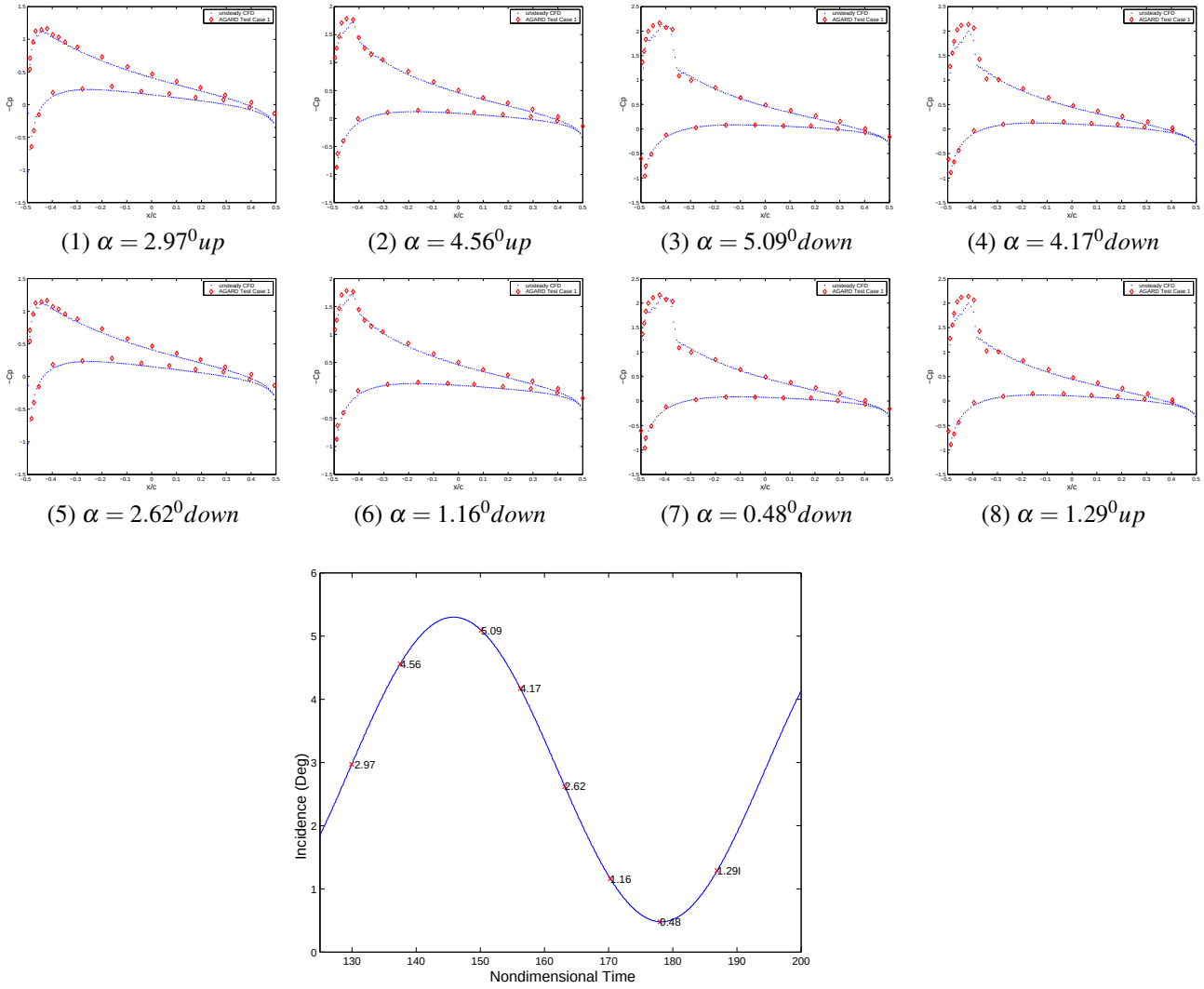

Figure 3 – Instantaneous pressure distributions for NACA0012 - AGARD test Case 1 (CT1)

Normal force (C_N) and moment coefficient (C_m) are obtained for three AGARD test cases the results on the three mesh refinement (Tab. 2). The meshes in the present work were generated with the commercial generator ICEM CFD, a very powerfull tool capable of creating sophisticated with very good refinament and grid quality control. The loops for C_N and C_m are shown in Fig. 4. For case CT5, the moment coefficient is obtained about the airfoil quarter chord, whereas for case CT1 and CT2 the moment coefficient is calculated about 0.273 chord. It was indicated in previous numerical studies Dubuc et al. (1997) that better agreement for the moment coefficient loop was obtained by using this corrected value, suggesting a possible error in the location of the moment center quoted for the experiments. The present results are in good agreement compared to the experiments, although it is clear that its value is also affected by the fact that the viscous effects have been neglected here when they might not be completely insignificant. Here, C_n and C_m results were also

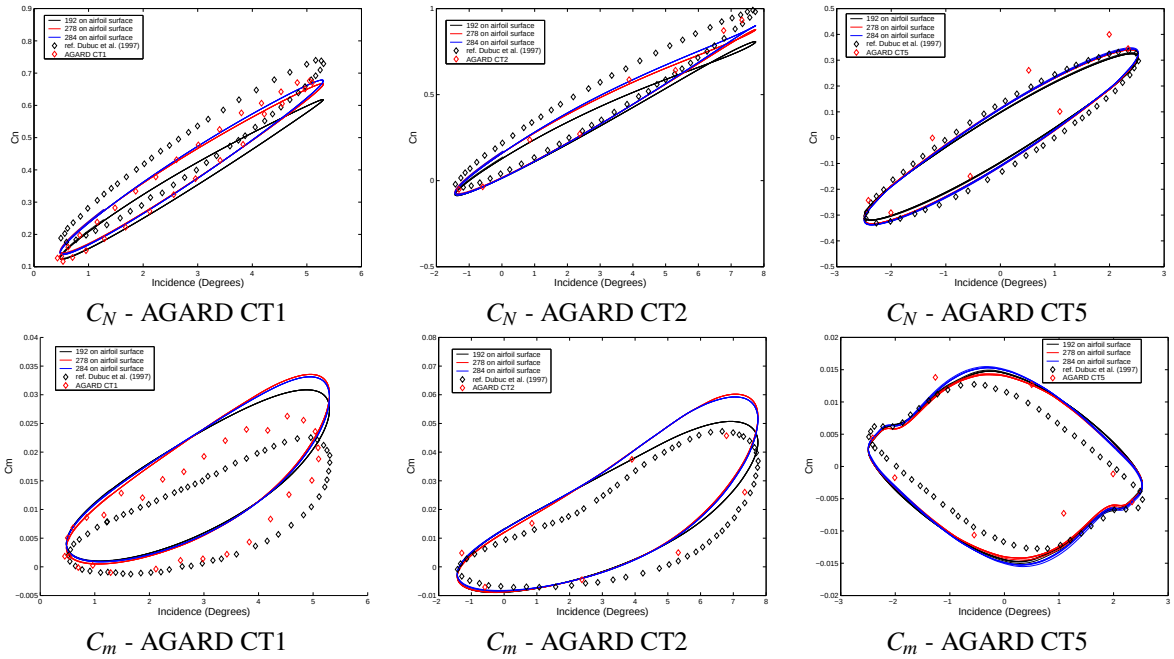

C_N - AGARD CT1 C_N - AGARD CT2 C_N - AGARD CT5

C_m - AGARD CT1 C_m - AGARD CT2 C_m - AGARD CT5

Figure 4 – Effect of grid refinament on solution

compared with implicit dual-time CFD methods given by Dubuc, et al. (1997). Differences between implicit dual-time CFD methods (Dubuc, et al., 1997) and present CFD code was observated. However, such discrepancies also appeared compared with experiments in the normal force.

Table 2 – Grids used for the grid refinament study.

Grid name	Grid size	Numder of points on airfoil surface
grid1	13744 volumes	192 points
grid2	15874 volumes	278 points
grid3	17844 volumes	284 points

Figure 4 shows also the corresponding normal force and moment coefficient for three grids considered here. The results exhibits a sensitivity to the size of the grid employed. However, these results suggest that gain in accuracy is obtained when using fine grids, and that sufficient accuracy can be obtained on a relatively coarse grid for Euler computation at similar flow conditions

Comparison of Stability Boundaries

The subsequent aeroelastic response of the model was obtained by a time marching solution of the aeroelastic equations (Eqs. (14)). The coupled computational fluid dynamic (CFD) and computational structural dynamics (CSD) method to the two-dimensional typical section was performed. It consists of a NACA0012 airfoil. The results were calculated using grid2 (Tab. 2) by first computing a converged steady flow solution about the airfoil with angle 0.1 degree of pitching about the elastic axis. The steady Euler solution was determined using the steady portion of the original unsteady Euler solver.

Time integration of the coupled fluid-structural equations of motion (Eq. (14) is applied and incorporated within the CFD Euler code as follows:

1. At time level n, perform an iteration of the Euler equation and calculate values for C_L and C_m;
2. This information is used by the equations of motion, to determine the position and velocity of the airfoil;
3. The new position and velocity are taken into account by the flow equations, and the process is repeated.

The test problem considered to illustrated the performance of the proposed scheme is for the NACA0012 airfoil. Time-marching aeroelastic analysis presented in this work is compared to the heavy case given by Hopf bifurcation analysis in Badcock, Woodgate and Richards (2004) shown in Fig 5. The parameters for the structural linear model are given in Tab.3. In the Badcock, Woodgate and Richards (2004), direct calculation of Hopf bifurcation points (flutter point) for an airfoil moving in pitch and plunge in transonic flow at zero incidence is considered. The iteration scheme for solving the Hopf equations is based on a modified Newton's method.

Table 3 – Structural model parameters

Parameter	Value
x_α	0.2
r_α^2	0.2905
$\bar{\omega}$	0.343
μ	100
a	-0.1

Here, time-marching analysis is at 0.1 initial incidence. Discrepancies can be observed when compared with Hopf's case, possibly due to the different initial incidence and mesh density used in calculations. In present work, for $M = 0.65$ up to approximately $M = 0.8$ the responses presented differents equilibrium points probably due to 0.1 initial incidence. Some difficulties were encountered with the exactly calculation of the flutter point. The flutter boundary shown in Fig. 5 of the present time-marching method were obtained when the system beginning limit cycle oscillations responses. Then, the results value is also affected by the possible wrong prediction of flutter point.

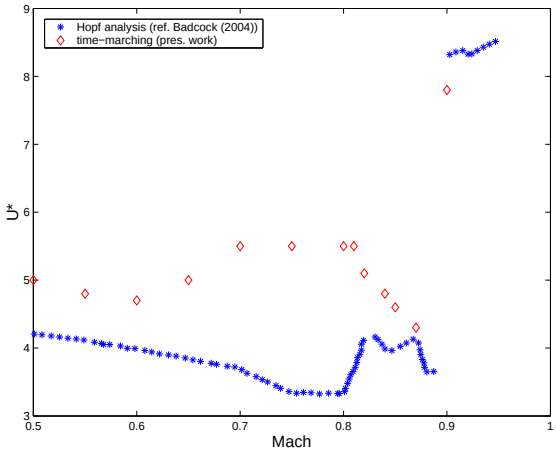

Figure 5 – Flutter boundary.

Effect of Torsional Free-play

To examine the effect of structural free-play on transonic flutter about the NACA0012 airfoil the structural parameters given in Tab.3 was utilized.

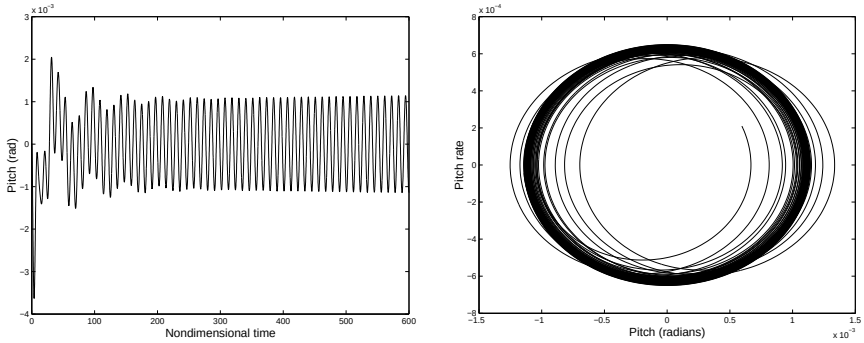

Time history Phase plane

Figure 6 – Pitch limit cycle for $U^* = 4.5$ without free-play.

First, at a constant Mach number 0.87, a series of time integration was performed at increasing reduced velocities without free-play. An example of this case is show in Fig. 6, which shows the pitch time history and phase plane plots for the case $U^* = 4.5$. The slow approach of the system to relatively small-amplitude limit cycle indicating linear flutter point (wich was found to be approximately 4.3. However, most of the runs do not need computations for many time periods, because system oscillations were easy identified with converging (*cf.* Fig. 7(a)) or diverging (*cf.* Fig. 7(b)) amplitude by

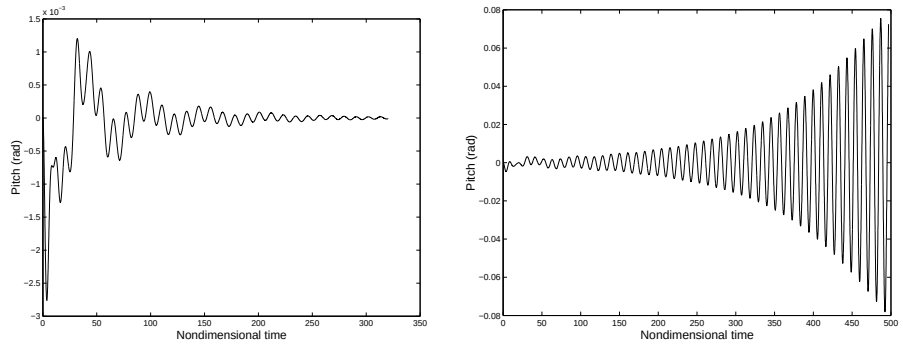

Time history Time history

Figure 7 – Pitch limit cycle for (a) $U^* = 4$ and (b) $U^* = 5$ without free-play.

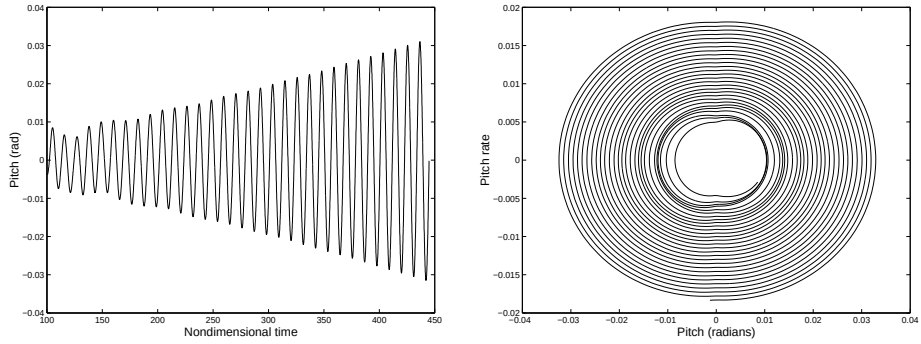

Time history Phase plane

Figure 8 – Free-play pitch limit cycle for $U^* = 4.5$.

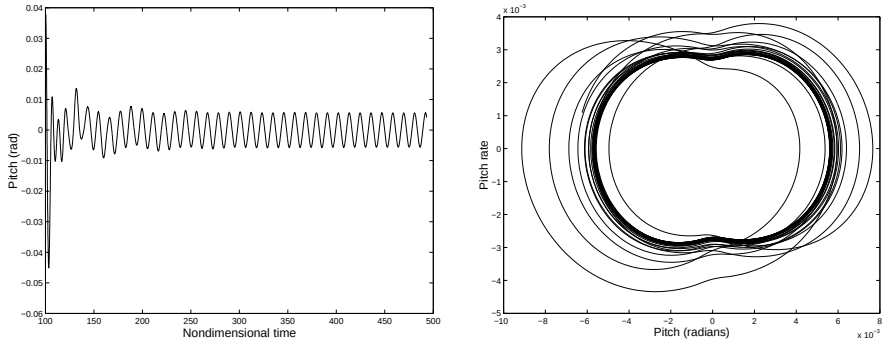

Time history Phase plane

Figure 9 – Free-play pitch limit cycle for $U^* = 4$.

looking at only few of them.

Free-play was then added to the torsional spring by setting $\alpha_s = 0.03$ deg, and the new coupled system was integrated forward in time for a range of U^* values. Some results for this situation are shown in Figs. 8 to 12. Figure 8 shows the pitch time history and phase plane trajectory for a reduced velocity of 4.5. Note that, in comparison with the linear structural response (*cf.* Fig. 6) the system with free-play presented divergent response.

Decreasing U^* in order to locate the stability point resulted in limit cycles of lesser amplitudes at reduced velocities of 4 (*cf.* Fig. 9), 3.5 (*cf.* Fig. 10) and 3(*cf.* Figs. 11). In all cases, the initial forcing amplitude of the airfoil was from 0.1 deg to guarantee that the system began its released oscillations outside the free-play region.

Figure 11 shows pitch time history and phase plane for reduced velocities of 2, the system does not enter a limit cycle, but to the stable equilibrium position.

Note that the flutter point of the system has dropped signicantly, from U^* about 4.5 without free-play, to around 3 with the free-play. In this sense, the addition of free-play has been highly destabilizing. A similar case to an NACA64A010 was observed in Kousen and Bendiksen (1994).

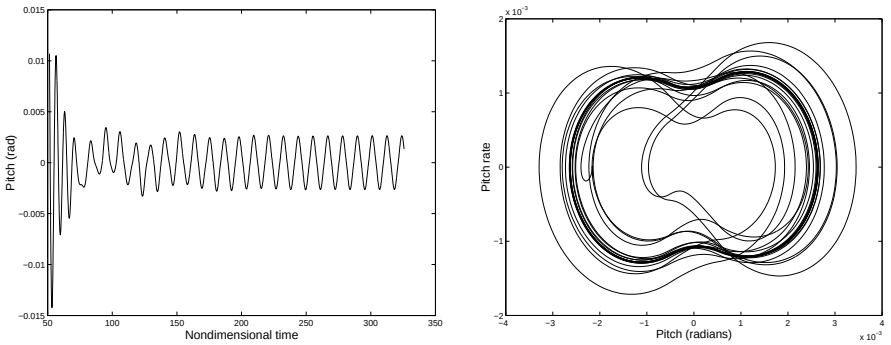

Time history Phase plane

Figure 10 – Free-play pitch limit cycle for $U^* = 3.5$.

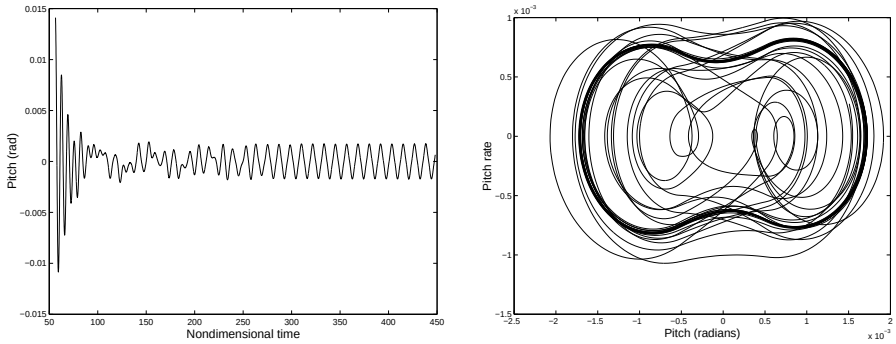

Time history Phase plane

Figure 11 – Free-play pitch limit cycle for $U^* = 3$.

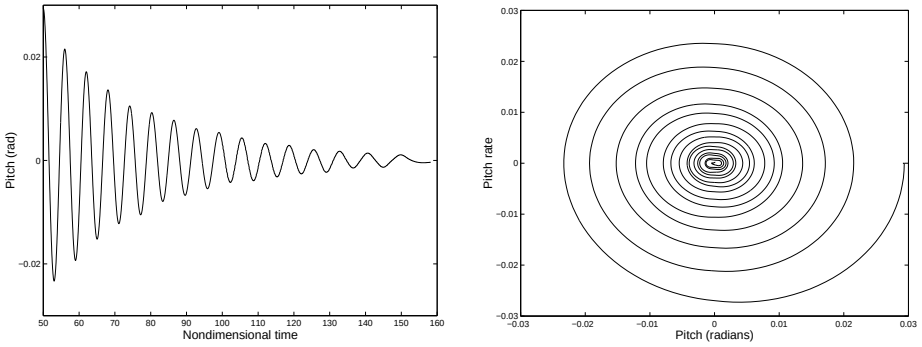

Time history Phase plane

Figure 12 – Free-play pitch limit cycle for $U^* = 2$.

CONCLUSIONS

The time marching aeroelastic analysis has been tested on a symetric pitch plunge airfoil problem. The unsteady analysis confirm the applicability of the CFD code for time stepping strategy and the effect of mesh refinement on solution.

The stability boundary on the medium grid was carried out and shows discrepencies compared with Hopf bifurcation method for flutter boundary given by Badcock, Woodgate and Richards (2004). To verify the time-integration aeroelastic algorithm, is necessary to consider the effect of grid refinament and time-marching aeroelastic calculations for the NACA0012 airfoil at zero initial incidence.

Adding torsional free-play to a typical section model in transonic flow proved strongly destabilizing. In the case studied, the linear structural flutter speed decreased and limit cycle amplitudes for U^* values above the flutter point were larger than the corresponding cases without free-play. These tests cases have presented the capability of the integrate CFD and structural program to predict nonlinear effects like LCO. However, the free-play is a discountinuous nonlinearity it is crucial that the system be integrated to the exact point where the change in stiffness occurs. In this sense, next steps with free-play nonlinearities will concentrate a similar state-space model to be developed using an alternative integration

scheme.

The validation of the present method for time-integration aeroelastic analysis represents only an intermediated step in the developement of a general nonlinear tools capable to study aeroelastic stability problems using modern CFD codes. During this development, Hopf bifurcation analysis for flutter boundary on transonic flow will be considered. This work developments will provide the basis for further advance to complete analysis of stability and bifurcation like LCO and chaos on transonic regime.

REFERENCES

Alonso, J. J. and Jameson, A., 1994, "Fully-implicit time-marching aeroelastic solutions", 32nd AIAA, Aerospace Sciences Meeting & Exhibit, 32 nd, Reno, NV.

Azevedo, J.L.F., 1992, "On The Development of Unstructured Grid Finite Volume Solver for High Speed Flows", *Report NT-075-ASE-N/92*, Instituto de Aerontica e Espa, S Josdos Campos, SP, Brazil.

Badcock, K. J.; Woodgate, M. A.; Richards, B. E., 2004, "Hopf Bifurcation Calculations for Simmetric Airfoil in Transonic Flow",*AIAA Journal*, vol. 42, n. 5, pp. 883-892.

Badcock, K. J.; Woodgate, M. A.; Richards, B. E., 2005, "Direct Aeroelastic Bifurcation Analysis of a Simmetric Wing Based on Euler Equations",*Journal of Aircraft*, vol. 42, n. 3.

Bigarella, E. D. V.; Basso, E.; Azevedo, J. L. F., 2004, "Cetered and Upwind Multigrid Turbulent Flow Simulations with Applications to Launch Vehicles", AIAA Paper 2004-5384, 22nd AIAA Applied Aerodynamics Conference and Exhibit, Providence, RI.

Bisplinghoff,R. L. and Ashley,H. and Halfman,R. L., 1996, "*Aeroelasticity*", Dover - New York.

Camilo, E. ; Marques, F. D. ; Azevedo, J. L. F., 2005, "Nonlinear Phenomena in Computational Transonic Aeroelasticity". In: 18th International Congress of Mechanical Engineering - COBEM 2005, Ouro Preto - MG/ Brazil.

Camilo, E. ; Marque, F. D. ; Azevedo, J. L. F., 2006, "Aeroelastic analysis of typical sections with structural and aerodynamic nonlinearities". In: 25th International Council of the Aeronautical Sciences - ICAS 2006, Hamburgo - Alemanha.

Dowell, E. H. and Tang, D., 2002, "Nonlinear aeroelasticity and unsteady aerodynamics", *AIAA Journal*, vol. 40, n. 9, pp. 1697-1707.

Dowell, E. H. and Tang, D. and Strganac, T. W., 2003, "Nonlinear aeroelasticity", *Journal of Aircraft*, Vol. 40, n. 5, pp. 857-874.

Dubuc L.; Cantarini F.; Woodgate, M. A.; Gribben B.; Badcock, K. J.; Richards, B. E., 1997, "Solution of the Euler Unsteady Equation Using Deforming Grids", Glasgow University Department of Aerospace Engineering, Report 9704.

Jameson, A. and Schmidt, W. & Turkel,E., 1981, "Numerical simulation of the euler equation by finite volume using Runge-Kutta time stepping schemes", AIAA Paper, pp. 81-1259.

Kousen, K. A. and Bendiksen, O. O., 1994, "Limit cycle phenomena in computational transonic aeroelasticity", *Journal of Aircraft*, vo. 32, n. 2, pp. 1257-1263.

Ko,J. and Kurdila,A. J. and Strganac,T. W., 1997, "Nonlinear dynamics and control for a structurally nonlinear aeroelastic system", Published by the American Institute of Aeronautics and Astronautics.

Lee, B. H. K. and Price, S. J. and Wong, Y. S., 1999, "Nonlinear aeroelastic analysis of airfoils: bifurcation and chaos", Progress in Aerospace Sciences, Vol.35, pp. 205-334.

Liu, F. and Cai, J. and Zhu, Y. and Tsai, H. M. and Wong, A. S. F., 2001, "Calculation of wing flutter by a coupled fluid-structure method", *Journal of Aircraft*, vol. 38, n. 2, pp. 334-342.

Morton, S. A., 1996, "Nonlinear Analysis of Airfoil Flutter at Transonic Speeds", Ph.D. Dissertation, Air Force Institute of Technology, Wright-Patterson AFB, OH.

Morton, S. A.; Beran P. S., 1999, "Hopf-Bifurcation Analysis of Airfoil Flutter at Transonic Speeds", *Journal of aircraft*, vo. 36, n. 2.

Oliveira, L. C., 1993, "A state-space aeroelastic analysis methodology using computational aerodynamics techniques", Master Thesis - Instituto Tecnolico de Aerontica, S Josdos Campos, S. P., Brazil, (in Portuguese).

Simoes, C. F. C.; Azevedo, J. L. F., 1999, "The influence of numerical parameters on unsteady airfoil inviscid flow simulations using unstructured dynamic meshes", Brazilian Progress in Aeroespace Engineering, uas de Linda, S Paulo, Brazil.

Thomas, J. P. and Dowell, E. H. and Hall, K. C., 2002, "Nonlinear inviscid aerodynamic effects on transonic divergence, flutter, and limit-cycle oscillations", *AIAA Journal*, vol. 40, n. 4, pp. 638-646.

RESPONSIBILITY NOTICE

The author(s) is (are) the only responsible for the printed material included in this paper.